Magnetic Field Overlying Solar Eruption Regions and Kink and Torus Instabilities

Y. Liu[1]

ABSTRACT

Using a Potential Field Source Surface model (PFSS), we study magnetic field overlying erupted filaments in solar active regions. The filaments studied here were reported to experience a kink instability or a torus instability. The torus instability leads to a full eruption, while the kink instability leads to a full eruption or a failed eruption. It is found that for full eruption the field decreases with height more quickly than that for failed eruption. A dividing line between full eruption and failed eruption is also found to be likely connected with the decay index n of the horizontal potential field due to sources external of the filament ($n = -d\ log(B_{ex})/d\ log(h)$, where h is height): the decay index of failed eruption tends to be smaller than that of full eruption. The difference of the decay indexes between full eruption and failed eruption is statistically significant. These are supportive of previous theoretical and numerical simulation results. Another significant difference is the field strength at low altitude: for failed eruption, the field strength is about a factor of 3 stronger than that for the full eruption. It suggests that the field strength at low altitude may be another factor in deciding whether or not a full eruption can take place. On the other hand, the decay index for the torus-instability full eruption events exhibits no trend to exceed the decay index for the kink-instability full eruption events on average, different from a suggestion derived from some MHD simulations. We discuss possible reasons that may cause this discrepancy.

Subject headings: Sun: activity; Sun: coronal mass ejections (CMEs); Sun: magnetic fields

1. Introduction

Kink and torus instabilities are suggested to be two mechanisms for triggering solar flares and Coronal Mass Ejections (CMEs) (Sakurai 1976; Török & Kliem 2005; Kliem &

[1]W. W. Hansen Experimental Physics Laboratory, Stanford University, Stanford, CA94305-4085

Török 2006). Recent MHD simulations indicate that the gradient of magnetic field overlying the erupted flux ropes is an important factor in deciding which instability actually takes place (Kliem & Török 2006; Fan & Gibson 2007), and whether or not a kink instability can eventually develop a successful eruption (Török & Kliem 2005). With MHD simulation, Török & Kliem (2005) modeled a failed eruption of a flux rope led by kink instability. When modified the overlying field to decrease with height more quickly, they found this flux rope eventually developed a full eruption. They thus concluded that "the decrease of the overlying field with height is a main factor in deciding weather the instability leads to a confined event or a CME." The simulation carried out by Fan & Gibson (2007) indicates that, for a kink-instability eruption, the overlying arcade field should decline with height more slowly than that for a torus-instability eruption. They suggest that slow decrease of overlying arcade field with height helps confine the flux rope so it can accumulate sufficient self-helicity for developing a kink instability. If we put these simulations together, we would expect to see a slow decrease of overlying field with height for a confined event of kink instability (or failed eruption. We denote this type of events as *FE* hereafter), a steep gradient of the overlying field for a full eruption of kink instability (We denote this type of eruptions as *KI* hereafter), and an even steeper gradient for a full eruption of torus instability (We denote this type of eruptions as *TI* hereafter).

In this work, we collect a sample of these three types of events from literature and study the magnetic field overlying the erupted regions. The purpose is to examine the characteristic of the field profiles for these three types of eruptions, as indicated by these MHD numerical simulations. The paper is organized as follows. In Section 2, we describe the events and calculation. The results are presented in Section 3. We conclude this research in Section 4.

2. Events and analysis

The events we choose for this research are erupted filaments in solar active regions, including four *FE* events from Green et al. (2007), four *KI* events from Williams et al. (2005) and Green et al. (2007), and two *TI* events from Schrijver et al. (2008). All the events in Williams et al. (2005) and Green et al. (2007) exhibit a clearly helical shape when erupted, suggesting a kink-instability eruption. Green et al. (2007) also showed that the events they analyzed have the same sign between the magnetic self-helicity of the erupted filaments (twist of flux tubes) and the rotation of the filaments (a proxy of writhing of flux tubes). This is strong evidence indicating development of a kink instability. For the two *TI* cases in Schrijver et al. (2008), numerical simulation of a torus instability shows a relatively close quantitative match of the data, implying that these two cases are likely to

be torus-instability eruptions.

The overlying magnetic field was computed from the observed magnetic field over the Sun's surface based on a Potential Field Source Surface model (PFSS) (Schatten et al. 1969; Altschuler & Newkirk 1969; Hoeksema et al. 1982; Wang and Sheeley 1992). In this model, it is assumed that the magnetic field is potential everywhere between the photosphere and a spherical source surface. The modeled field matches the radial component on the photosphere and is forced to become purely radial on the source surface. In this work, the source surface is set at 2.5 radii from Sun center. We use synoptic frame, a special type of synoptic maps of magnetic field, as the input to compute the potential field. A synoptic frame is generated by combining the traditional Carrington synoptic charts and a full disk magnetogram taken at the time of interest (Zhao et al. 1997). This full disk magnetogram, being remapped onto the heliographic coordinates first, is inserted into the synoptic charts. The synoptic frame is thus deemed to approximate the distribution of magnetic field over the entire solar surface at the time of the magnetogram. The magnetograms used were observed by SOHO/MDI (Scherrer et al. 1995) at the times close to the events. The field overlying the erupted filaments is estimated from the computed potential field. Since the filaments are usually observed to lie along the magnetic neutral lines, the field strength at each height is computed by averaging the horizontal field along the magnetic neutral line between the major opposite polarity patches of the active region where the eruption took place. Note that in the theoretical work of Kliem & Török (2006) the field used to derive the profile is the poloidal component of the external potential field only, while here the field analyzed includes both poloidal and toroidal components. This is appropriate since many of the erupting filaments rotated and so effectively felt a combination of both components.

To quantitatively compare the field profiles of those events, following Török & Kliem (2007), we also compute the decay index of the external field, represented by the horizontal components of our PFSS model, n, assuming $B_{ex} \propto h^{-n}$, where h is height. Figure 1 shows an example of how to calculate the decay index. The event occurred on June 6, 2000 (event 1 in Table 1). The y-axis represents strength of horizontal magnetic field, while the x-axis represents the height measured from the photosphere. The height ranges from 42 Mm to 105 Mm. We choose 42 Mm for the starting height, the average of the initial heights from four events (events 2, 3, 9 and 10) for which the initial heights were obtained from observation (Schrijver et al. 2008; Ji et al. 2003; Romano et al. 2003). The strength and height are in logarithm. The decay index is the slope from the linear fitting to the data, as shown in the Figure.

Listed in Table 1 is a summary of the events. We include a second decay index in the summary, computed by averaging the horizontal component of magnetic field over the whole

area of the active regions where the eruptions took place. The resulting decay index n_2 and field strength B_{t2} are lower, and the scatter of n_2 tends to increase. This indicates that the derived decay index from neutral line data, n_1, is more accurate. In the following sections, we will only use n_1 for analysis unless otherwise specified.

3. Results

A clear dividing line between *FE* and full eruption (both *KI* and *TI*) appears to be connected with the decay index: n_1 is less than 1.71 for *FE* and greater than 1.74 for *KI* and *TI*. This trend is further confirmed by the plot in Figure 2. Plotted in Figure 2 is magnetic strength as a function of height. Both strength and height are in logarithm. For comparison, we shift the curves in y-axis so that they all have the same maximum value. It is seen that the field for *FE* (green curves) tends to decrease with height more slowly than that for *KI* (red curves) and *TI* (black curves). This supports the theoretical and MHD simulation results (Török & Kliem 2005; Kliem & Török 2006). In high altitude, however, the field for *FE* declines with height more quickly than that for *KI* and *TI* (see Figure 3), indicating that the field immediately above the filaments is more important than the field at high altitude to decide whether a confined event or a CME occurs.

To make a more quantitative comparison, we average the parameters for each type of eruption (see Table 2). We also included *KI* and *TI* together as a type of full eruption (the bottom row in Table 2) in order to compare with the failed eruption (*FE*). Basically, the decay index for *FE* is smaller than that for *KI* and *TI*. It is confirmed by a 90% confidence test that clearly discriminates the decay indexes between failed eruption and full eruption. A critical decay index was suggested theoretically to range from 1.5 to 2.0 (Kliem & Török 2006), while MHD simulations gave a value of 1.53 (Török & Kliem 2005) and 1.9 (Fan & Gibson 2007) for a full eruption of flux rope. In this study, the average of decay index for *KI+TI* is at the upper end of this range, and the index for *FE* is at the lower end. No decay indexes are smaller than the lower limit of the critical value for full eruption events, nor do any exceed the upper limit for the failed eruption events (See Table 1). These results are supportive of the previous theoretical and simulation results (Török & Kliem 2005; Kliem & Török 2006; Fan & Gibson 2007).

Another outstanding difference between *FE* and *KI+TI* is the strength of horizontal field at low altitude: at a height of 42 Mm, the average of initial height of erupted filaments, the strength for the failed eruption events is about a factor of 3 stronger than that of full eruption events. It suggests that the magnetic strength in low altitude is probably another main factor in deciding whether a full eruption or a failed eruption eventually takes place.

In a detailed analysis of a failed eruption of a filament, Ji et al. (2003) reported that the erupted filament reached a maximum height of 80 Mm before falling back to the Sun. The deceleration of the filament is estimated to exceed the gravitational deceleration by more than a factor of 10, suggesting that the strong closed field at low altitude pulled the filament material back down.

The difference of magnetic strength between *FE* and *KI+TI* is probably due to the size of the active regions. The total flux of the active regions for *FE* are about a factor of 3 greater than that for *KI+TI* (see Table 2). It suggests that the *FE* events tend to occur in big active regions. Big active regions usually produce more CMEs. We thus speculate that either kink and torus instabilities are not the mechanisms for those eruptive events, or that the instabilities can lead to these events only if they occur high enough where the decay index becomes sufficient large (see Figure 2).

KI and *TI* events show a rather similar decrease of the overlying field on average (see Figure 2). Consistently, the decay indexes for *KI* and *TI* are also similar on average (see Table 2). This does not support the suggestion of a steeper decrease for *TI* events in Fan & Gibson (2007). This needs further investigation after more events are collected, because in this research, the sample of *TI* is too limited, and the data used here poorly represents the field at the times when the events occurred. So far, we only analyzed two *TI* events that have a time interval of 4 and 5 days, respectively, between the inserted full-disk magnetogram and the eruptive event. The active region fields could evolve substantially in such a long time interval.

4. Conclusions

In this research, we have studied profile of magnetic field overlying solar eruption regions, in order to observationally examine their characteristics for the three types of eruptions, *TI, KI* and *FE*, as predicted by the numerical simulations. The events studied here are erupted filaments in solar active regions, including four *FE* events, four *KI* events and two *TI* events. It is indicated that the field decreases with height more slowly for *FE* than for *KI* and *TI*. The decay index of *FE* is also consistently smaller than that of *KI* and *TI*. The difference between them is statistically significant. A dividing line between *FE* and *KI+TI* appears to be related to the decay index: no decay indexes for *FE* exceed 1.71 and no decay indexes for *KI+TI* are smaller than 1.74. For *FE*, the average of the decay index is at the lower end of the range of the theoretically proposed critical index and at the upper end for *KI+TI*. These are supportive of the theoretical and numerical results (Török & Kliem 2005; Kliem & Török 2006; Fan & Gibson 2007).

Another significant difference between *FE* and *KI+TI* is the horizontal magnetic field at low altitude. The strength for *FE* is about a factor of 3 stronger than that for *KI+TI*. It suggests that the field strength at low altitude may be another factor in deciding whether or not a full eruption should take place, in addition to the gradient of magnetic field overlying the erupted flux ropes as suggested by the MHD simulations.

KI and *TI* events show a rather similar decrease of the overlying field with height on average. This does not support the suggestion by the MHD simulation (Fan & Gibson 2007), which indicates that the field decreases with height more slowly for *KI* than that for *TI*. Large time interval between the events and the data used for modeling coronal field may be one reason for this discrepancy. It will be further investigated after more events are collected.

The author wish to thank the referee, Dr. B. Kliem, for constructive comments and suggests that help improve this work substantially. The author thanks X. Zhao at Stanford University for providing the PFSS code. This work was supported by the NASA NAG5-13261, and NSF/CISM project under grant ATM-0120950. SOHO is a project of international cooperation between ESA and NASA.

REFERENCES

Altschuler, M. D., Newkirk, G., Jr. 1969, Sol. Phys., 9, 131

Fan, Y., Gibson, S. E., 2007, ApJ, 668, 1232

Green, L.M., Kliem, B., Török, T., van Driel-Gesztelyi, L., Attrill, G.D.R., 2007, Sol. Phys., 246, 365.

Hoeksema, J. T., Wilcox, J. M., Scherrer, P. H. 1982, J. Geophys. Res., 87, 10331

Ji, H., Wang, H., Schmahl, E. J., Moon, Y.-J., Jiang, Y. 2003, ApJ, 595, L135

Kliem, B., Török, T., 2006, *Phys. Rev. Lett.*, 96, 255002

Romano, P., Contarino, L., Zuccarello, F. 2003, Sol. Phys., 214, 313

Sakurai, T., 1976, *PASJ*, 28, 177

Schatten, K. H., Wilcox, J. M., Ness, N. F. 1969, Sol. Phys., 6, 442

Scherrer, P. H., Bogart, R. S., Bush, R. I. et al. 1995, Sol. Phys., 162, 129

Schrijver, C. J., Elmore, C., Kliem, B., Török, T., Title, A. M., 2008, ApJ, 674, 586.

Török, T., Kliem, B., 2005, ApJ, 630, L97

Török, T., Kliem, B., 2007, *Astronomische Nachrichten*, 328, 743

Wang, Y. -M., Sheeley, N. R., Jr. 1992, ApJ, 392, 310

Williams, D. R., Török, T., Demoulin, P., van Driel-Gesztelyi, L., Kliem, B. 2005, ApJ, 628, L163

Zhao, X. P., Hoeksema, J. T., Scherrer, P. H., 1997, in *The Fifth SOHO Workshop*, **SP-404**, p. 751.

Table 1: List of the events in this study

ID	Type[a]	Flare	Date, Time [b] (dd/mm/yy, UT)	AR	Flux[c] (e22) (Max)	Int.[d] (day)	n_1[e] (NL)	B_{t1}[f] (NL) (G)	n_2[g] (AR)	B_{t2}[h] (AR) (G)	Source [i]
1	FE	X1.1	06/06/00 1330	9026	5.93	0	1.51	58.4	1.15	33.1	G
2	FE		19/07/00 2330	9077	6.76	3	1.65	44.2	1.50	23.6	G
3	FE		27/05/02 1805	9957	6.98	2	1.71	51.3	1.45	28.9	G
4	FE	M1.0	02/05/03 0247	0345	6.71	0	1.62	99.3	1.56	60.0	G
5	KI	C6.8	07/04/97 1350	8027	1.12	0	1.75	12.6	1.41	7.3	G
6	KI	C1.3	12/05/97 0442	8038	0.88	0	1.88	12.3	1.66	7.0	G
7	KI	M6.3	15/06/01 0952	9502	1.99	0	1.85	28.3	1.75	20.4	G
8	KI	X2.5	10/11/04 0156	0696	4.65	2	2.25	35.9	2.09	20.1	W
9	TI	M4.0	16/06/05 1910	0775	3.70	5	2.04	26.4	1.72	11.6	S
10	TI	M3.7	27/07/05 0300	0792	4.56	4	1.74	33.0	1.43	18.1	S

[a] Types of eruption. *FE* denotes failed eruption of kink instability. *KI* means kink instability eruption. *TI* represents torus instability eruption.

[b] Date and time of the occurrence of flares.

[c] Total flux of the active region.

[d] Time interval between the occurrence of the event and the observational time of a full disk magnetogram that was used to generate the synoptic frame. The potential field is extrapolated from this synoptic frame.

[e] Decay index derived in the height range 42–105 Mm from the data averaged along the magnetic neutral line of the major opposite magnetic polarity patches of the active region on the photosphere.

[f] The average of the horizontal magnetic field at a height of 42 Mm, immediately above the filament's pre-eruption height. The average is done along the magnetic neutral line of the major opposite magnetic polarity patches on the photosphere.

[g] Decay index derived in the height range 42–105 Mm from the data averaged over the active region where the eruption took place.

[h] The average of the horizontal magnetic field at a height of 42 Mm. The average is performed over the whole area of the active region where the eruption took place.

[i] The source of the events. *G* denotes the events from Green et al. (2007). *W* denotes event from Williams et al. (2005). *S* denotes the events from Schrijver et al. (2008).

Table 2: Three types of eruption: average

Type	Flux (e22) (Max)	n_1 (NL)	B_{t1} (NL) (Gauss)	n_2 (AR)	B_{t2} (AR) (Gauss)
FE	6.60 ± 0.33	1.62 ± 0.05	63.3 ± 18.0	1.42 ± 0.13	36.4 ± 11.8
KI	2.16 ± 1.25	1.93 ± 0.15	22.3 ± 9.8	1.72 ± 0.19	13.7 ± 6.5
TI	4.13 ± 0.43	1.89 ± 0.15	29.7 ± 3.3	1.57 ± 0.15	14.8 ± 3.2
KI+TI	2.81 ± 1.48	1.91 ± 0.15	24.7 ± 8.2	1.67 ± 0.18	14.0 ± 5.4

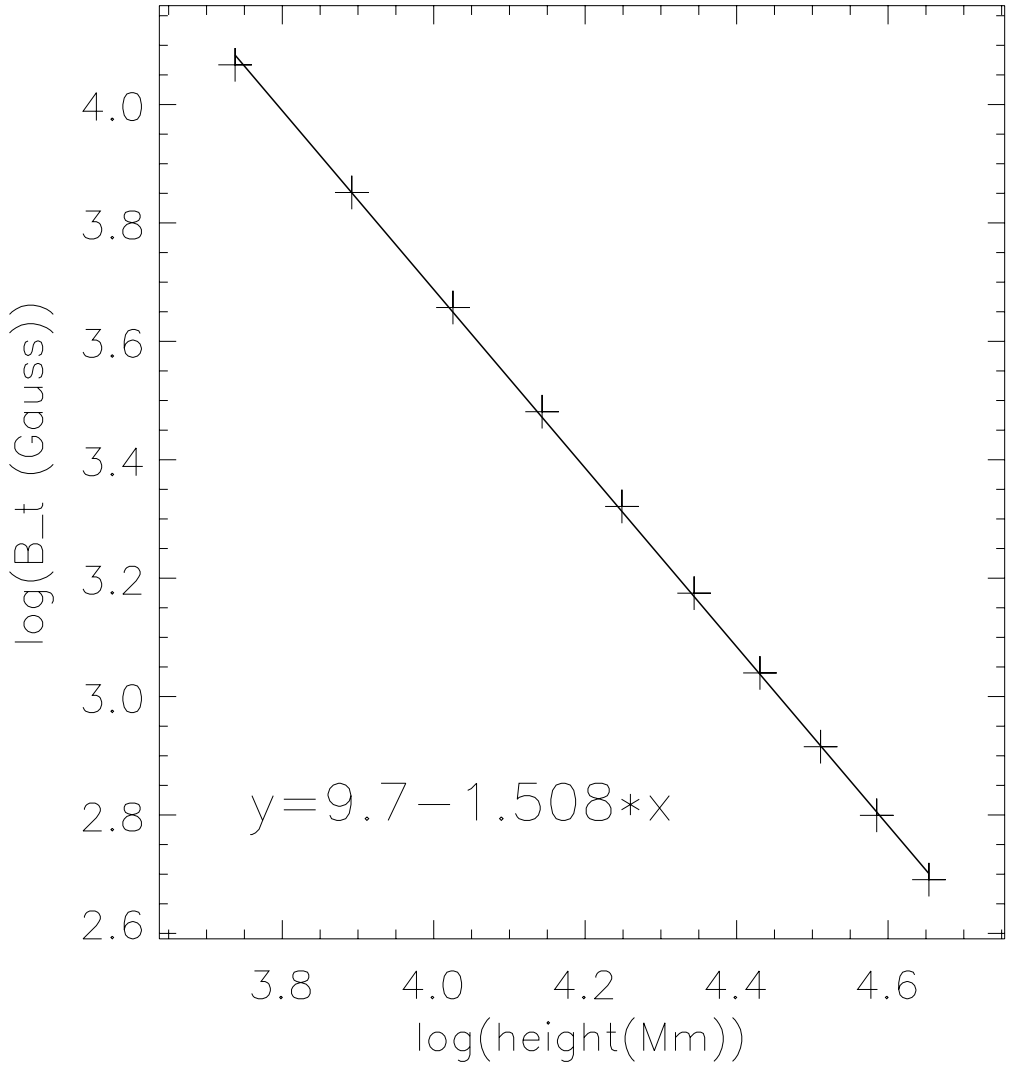

Fig. 1.— An example of fitting of magnetic field strength and height for the 2000 June 6 event. The strength and height are in logarithm. The height is measured from the photosphere. The range of the height is from 42 Mm to 105 Mm. The symbol of '+' represents calculated field while the solid line is the result of a linear fitting to the data. The slope here is actually the decay index detailed in the text.

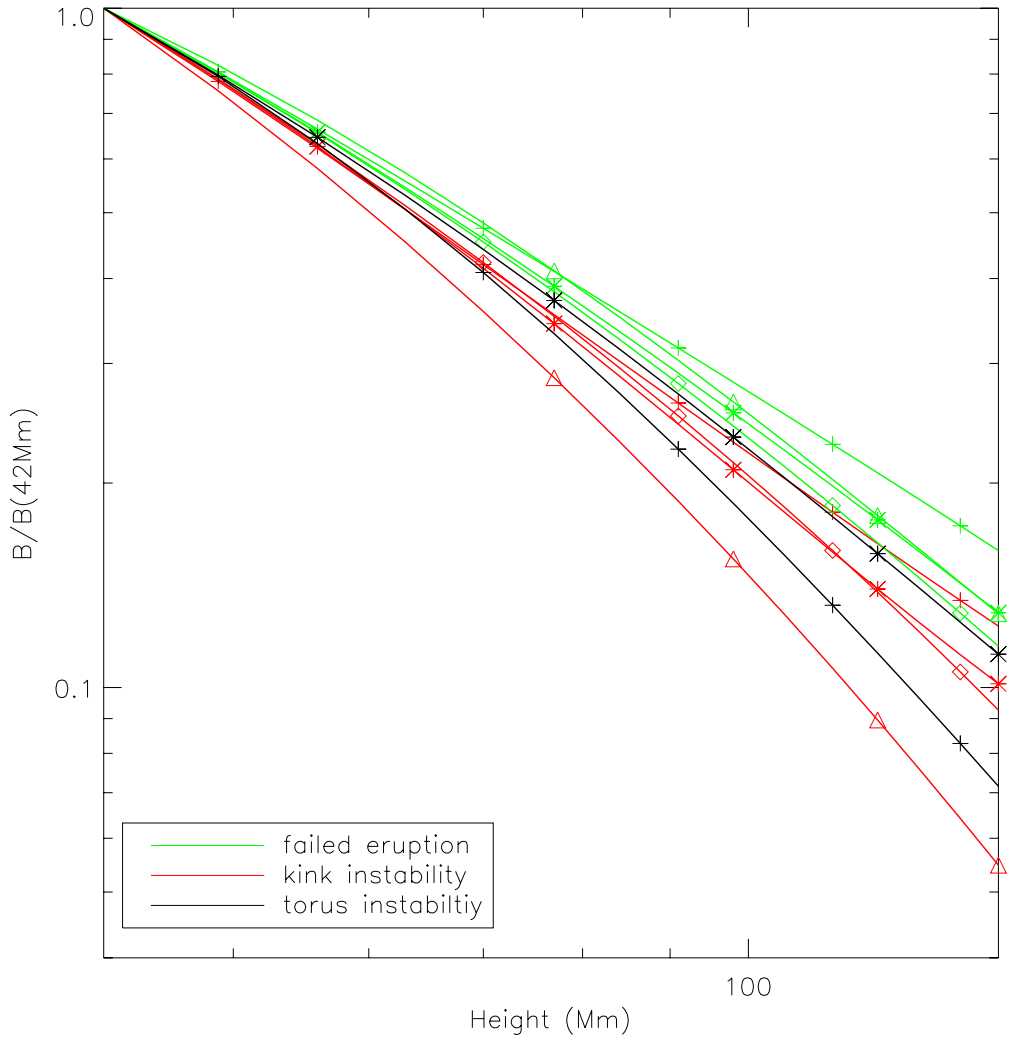

Fig. 2.— Profile of horizontal magnetic field above the erupted regions. The field is averaged along the magnetic neutral line of the active region where the eruption took place. This is a logarithm-logarithm plot. The green, red and black curves represent *FE, KI* and *TI*, respectively. The green and red curves with symbols cross, star, diamond and triangle represent events 1-4, and events 5-8, while the black curves with cross and star denote events 9 and 10 (see Table 1). The height is from 42 Mm to 140 Mm.

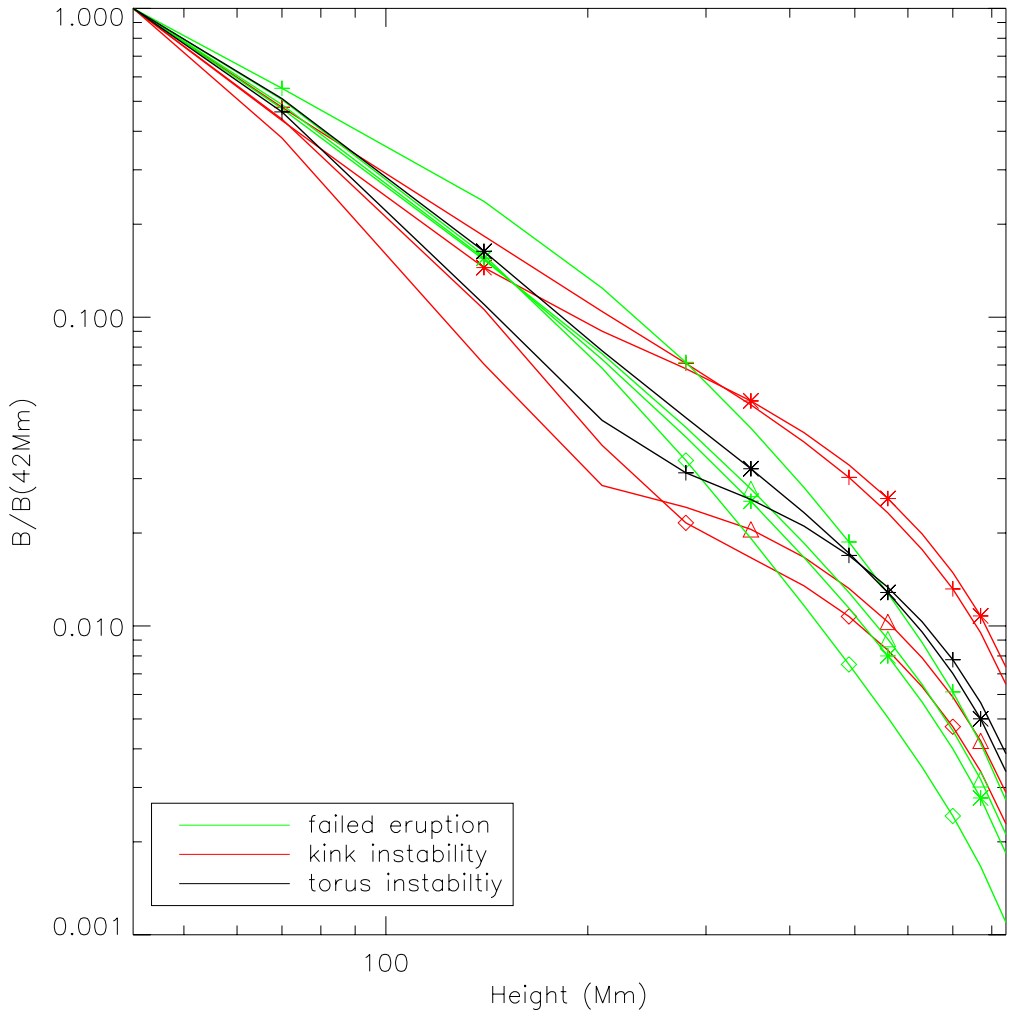

Fig. 3.— Horizontal magnetic field above the erupted regions as a function of height. The field strength and height are both in logarithm. The height ranges from 42 Mm to 840 Mm. The strength is computed by averaging the whole area of the active region where the eruption took place. Since we are going to examine behaviors of magnetic field at high altitude that is comparable with the size of active region, the field averaged over the whole active region is more appropriate. Again, as in Figure 2, the green, red and black curves represent *FE, KI* and *TI*, respectively, and the symbols denote each individual event.